Journal of Applied Mechanics and Technical Physics, Vol. 51, No. 1, pp. 4–10, 2010

PARAMETRIC STUDY OF UNSTEADY LAMINAR FLOWS

A. M. Lipanov and S. A. Karskanov

UDC 533.6:519.63

Results of a parametric study of unsteady laminar flows are analyzed. Three-dimensional unsteady equations of hydromechanics for a compressible medium are solved. The range of the characteristic Reynolds number $\mathrm{Re} = 400$–900 *is considered. It is demonstrated that the laminar flow in a plane channel ceases to be steady at* $\mathrm{Re} = 415$. *As the Reynolds number increases, the unsteady processes become more intense, disturbances penetrate inward the channel, and separation zones lose their stability. In the vicinity of the channel exit, however, the flow tends to stabilize, though it remains unsteady. No transition to a turbulent flow occurs in the examined range of Reynolds numbers.*

Key words: *equations of hydromechanics, Reynolds number, Mach number, Prandtl number, domain of integration, separation zone.*

In [1, 2], we studied parametrically steady laminar flows in a channel, which remain symmetric at Reynolds numbers $\mathrm{Re} \leqslant 90$ and acquire an asymmetric structure at $\mathrm{Re} > 90$; this effect is particularly noticeable in the vicinity of the channel entrance. Far from the channel entrance, this asymmetry disappears, and the flow becomes one-dimensional.

Results of a theoretical study of unsteady laminar flows are analyzed in the present paper.

In the vicinity of the Reynolds number $\mathrm{Re} \approx 400$, the steady flow loses its stability and becomes unsteady. Kochin et al. [3] assumed that this variant of the loss of stability is the transition to turbulence, but Fedorchenko [4] demonstrated that this is the transition to an unsteady laminar rather than turbulent flow. The transition to turbulence occurs at Reynolds numbers $\mathrm{Re} > \mathrm{Re}_{\mathrm{cr}}$.

As in [1, 2], we consider a system of unsteady three-dimensional equations of hydromechanics. The following dimensionless variables are used: the time t, the streamwise, vertical, and spanwise (transverse) spatial coordinates x, y, and z, which form the left-hand coordinate system, and hydromechanical parameters p, ρ, U, V, W, and E, which are the pressure, density, components of the flow velocity vector, and specific energy, respectively.

The problem is solved for a channel shown in Fig. 1. The coordinates x, y, and z correspond to the components U, V, and W of the flow velocity vector, respectively. The boundary conditions at the channel entrance are set in the plane of the vertical walls of the steps. The gas flows in a plane channel with Reynolds numbers $\mathrm{Re} = 400$–900 considered in the paper are typical for various engineering devices and test facilities (channels of gas-dynamic communication in flying vehicles, fans, turbines, wind tunnels, etc.).

The scaling quantities were the step length h equal to the channel width at the entrance for linear quantities, the maximum value of the streamwise component $U_\wedge$ of the flow velocity vector at the channel entrance for velocities, and the pressure $p_\wedge$ and density $\rho_\wedge$ corresponding to $U_\wedge$ for the pressure and density. Using these quantities, we obtained the Reynolds, Mach, and Prandtl numbers, assuming that $\mathrm{M} = 0.6$ and $\mathrm{Pr} = 0.7$. The viscosity $\mu = 2 \cdot 10^{-5}$ kg/(m·sec) and thermal conductivity $\lambda = 0.03$ W/(m·K) were assumed to be constant, because the level of temperatures in the problem was close to normal, and the temperature in this range of velocities remains almost unchanged.

Institute of Applied Mechanics, Ural Division, Russian Academy of Sciences, Izhevsk 426067; ipm@udman.ru; ser@udman.ru. Translated from Prikladnaya Mekhanika i Tekhnicheskaya Fizika, Vol. 51, No. 1, pp. 7–15, January–February, 2010. Original article submitted September 13, 2007; revision submitted February 25, 2009.

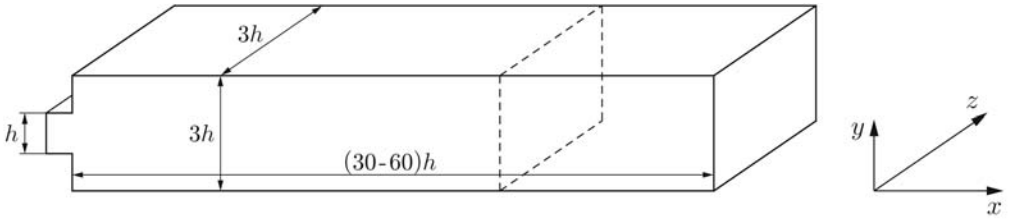

Fig. 1. Domain of integration.

We considered a subsonic flow in a channel of length $L = 60$ and height $2H = 3$ equal to the channel width. The difference grid consisted of 1,022,301 ($601 \times 81 \times 21$) nodes. This number of computational points of the difference grid was chosen for the error of the approximate solution to be smaller than 0.1%. The computations were performed on a multiprocessor computer system with 20 processors at the Interdepartmental Supercomputer Center of the Russian Academy of Sciences. The domain of integration was divided into identical subdomains in the x direction.

The equations of hydromechanics were integrated with respect to time by the second-order Runge–Kutta method. Integration with respect to spatial variables was performed with the eighth order of accuracy. Inside the domain of integration, the derivatives were approximated by the eighth-order central differences on a nine-point template. The derivatives near the boundaries were calculated from the values of internal points by the finite difference method, but the template was extended to ten points because of its asymmetry to preserve the eighth order of accuracy of integration in space. Diffusion terms containing second-order derivatives were calculated by formulas for the second derivatives. This method was described in more detail in [5], where it was demonstrated that the error of modeling a turbulent flow with $\mathrm{Re} = 10^4$ and $\mathrm{M} = 0.6$ in the same channel on the same spatial grid with the eighth order of approximation of derivatives in space and with the second order of approximation in time was smaller than 0.1%. The flows considered in the present paper are more ordered and have typical Reynolds numbers $\mathrm{Re} < 10^4$; in the present case, therefore, the accuracy of numerical results obtained is not worse.

The components U_0, V_0, and W_0 of the flow velocity vector were specified at the channel entrance. In this case, we have

$$U_0 = \varphi(y, \delta_U) + C_1(p_0 - \langle p \rangle)\varphi(y, \delta_S); \tag{1}$$

$$\varphi(y, \delta_\xi) = \begin{cases} 1 - (1 - y/\delta_\xi)^N, & 0 \leqslant y \leqslant \delta_\xi, \\ 1, & \delta_\xi < y \leqslant h - \delta_\xi, \\ 1 - ((y - h + \delta_\xi)/\delta_\xi)^N, & h - \delta_\xi < y \leqslant h, \end{cases}$$

where the subscript ξ acquires the values U and S (S is the entropy function), p_0 is the pressure at the channel entrance, which is obtained in the course of solving the problem, $\langle p \rangle$ is the mean pressure at the channel entrance (the averaging is performed only in the plane of the channel entrance where the boundary conditions are imposed), the coefficient C_1 is determined by the formula $C_1 = 1/(k\mathrm{M})$ ($k = 1.4$ is the ratio of specific heats), $\delta_U = 0.2$ and $\delta_S = 0.1$ are the dimensionless thicknesses of the dynamic and thermal boundary layers, and N is the order of approximation.

According to [4], the second term in condition (1) is used to move perturbations reaching the left (input) boundary of the channel outside the domain of integration. The components V_0 and W_0 are assumed to be equal to zero:

$$V_0 = W_0 = 0. \tag{2}$$

In addition, the isentropic condition is set for the flow core at the channel entrance:

$$p_0 = S_0 \rho_0^k.$$

In this case, the relation for calculating the dimensionless temperature with allowance for the presence of the boundary layer has the form

$$T = 1 + (S_0 p^{(k-1)/k} - 1)\varphi(y, \delta_S),$$

where S_0 is the dimensionless entropy function (in the calculations, we assume that $S_0 = 1$).

At the channel exit ($x = L$), we set the condition

$$p_L = p_{\text{ext}} + C_2(m_L - \langle m \rangle), \tag{3}$$

where $m = \iint\limits_{S(x)} \rho U \, dy \, dz$ is the mass flow of the gas through the x cross section of the channel at the current time, $\langle m \rangle = \dfrac{1}{L} \int\limits_0^L m \, dx$ is the mass flow at the current time averaged over the channel length, m_L is the mass flow at the channel exit, p_{ext} is the ambient pressure, i.e., external pressure (in dimensionless form, $p_{\text{ext}} = 1$), $C_2 = k\text{M}\,/(2H + \langle m \rangle \text{M}\,)$, and H is the channel half-height (in the y direction).

According to [4], the second term in condition (3) is used to move perturbations reaching the right (output) boundary of the channel outside the domain of integration. The remaining hydromechanical parameters at the output are determined by extrapolation with the use of "soft" boundary conditions.

On the wetted surfaces, which are considered as adiabatic surfaces, we impose the no-slip condition

$$U = V = W = 0$$

and the condition of adiabaticity

$$\frac{\partial T}{\partial n} = 0,$$

i.e., we consider temperature levels in a moving medium where heat exchange with the walls can be neglected.

One of the planes xy is chosen as the origin for the variable z. At a distance $\pm H_z$ from this plane, we set the periodicity conditions

$$U_+ = U_-, \qquad V_+ = V_-, \qquad W_+ = W_-, \qquad p_+ = p_-, \qquad \rho_+ = \rho_-.$$

The distance H_z is chosen by the trial method on the basis of asymptotic convergence with given accuracy of computations and is taken to be 1.5.

In addition, a three-dimensional perturbation is initiated at the channel entrance at the initial time. For this purpose, instead of conditions (2), we use the equalities

$$V_0 = W_0 = 0.1U_0.$$

Such a three-dimensional flow at the channel entrance is sustained during a certain time determined from a numerical experiment. Lipanov et al. [5] showed that 100 steps of integration with respect to time (0.2 dimensionless units) are sufficient for the flow to remain three-dimensional for an arbitrarily long time in computations within the turbulent range of hydromechanical parameters. If the third component W of the flow velocity vector decays, this means that the range of hydromechanical parameters considered is laminar.

After 100 steps of integration with respect to time, we again use conditions (2). At this instant, the dimensionless time is $t = 0.2$. Figure 2 shows the time evolution of the transverse (third) component W of the flow velocity vector in the channel at Re = 800. It is seen that the entire domain of integration with a length of 30 units is involved into motion at $t = 60$ (see Fig. 2b). The front of velocity perturbation located in the vicinity of the right boundary of the channel is fairly intense ($W = 0.002$), as compared with the perturbation front at $t = 28$ ($W = 0.003$) (see Fig. 2a). In the remaining volume of the channel, however, the perturbations are already two orders of magnitude less intense than at $t = 28$; therefore, the flow at $t > 60$ is two-dimensional even at Re = 800. This picture shows that the range of hydromechanical parameters is laminar, because three-dimensionality is one of the specific features of turbulent flows.

Figure 3 shows the streamlines at the time $t = 400$ at Re = 600. The gas motion is unsteady, and we see the formation of reverse flows not only in the vicinity of the channel entrance, but also further downstream to the value $x = 40$. The unsteady phenomena are manifested to the greatest extent near the left boundary of the channel: the separation regions are larger in size and contain several dividing and merging vortices. Beginning from $x = 17$, the separation regions contain only one large vortex each. Further downstream, at $x > 17$, the maximum transverse size of the separation regions gradually decreases. At sufficiently large values of x, the separation regions with reverse flows are periodically replaced by zones with slow motion, and the flow is slightly deflected above these

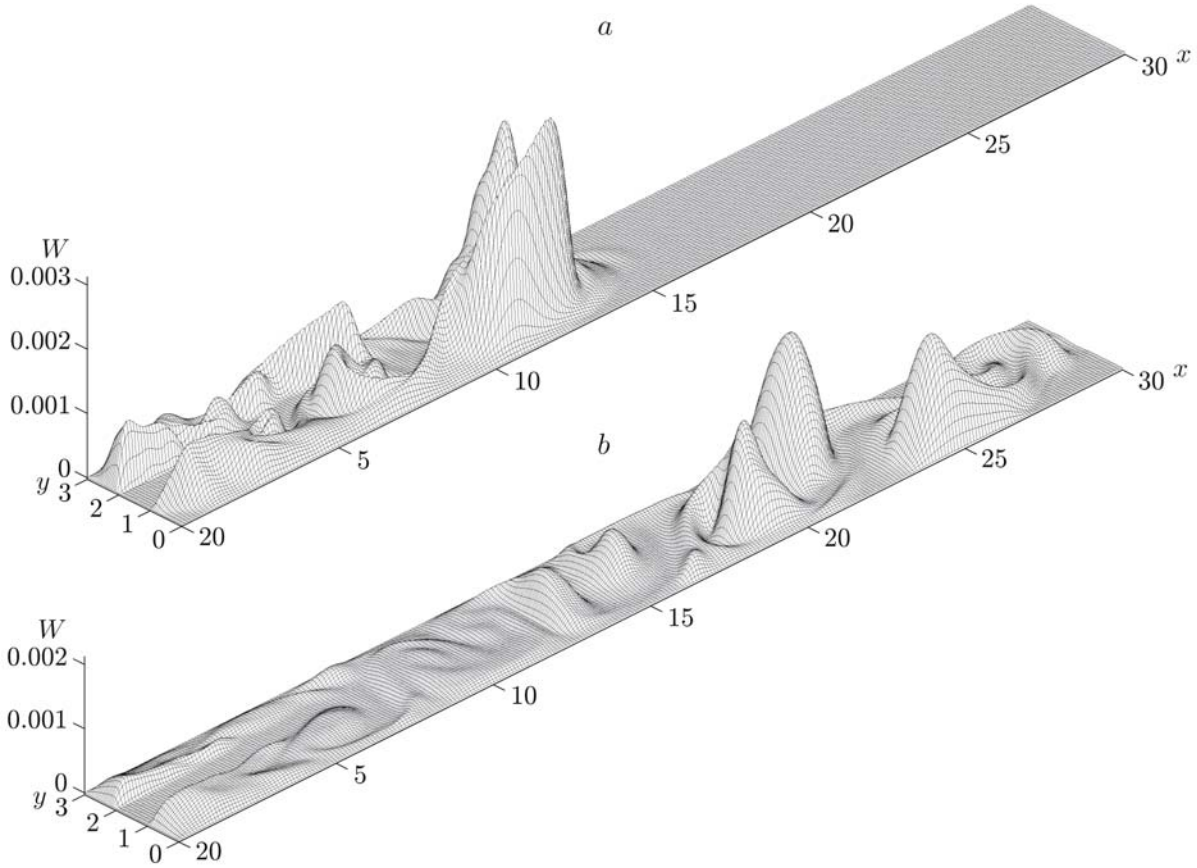

Fig. 2. Time evolution of the transverse (third) component W of the flow velocity vector at $\mathrm{Re} = 800$ and $t = 28$ (a) and 60 (b).

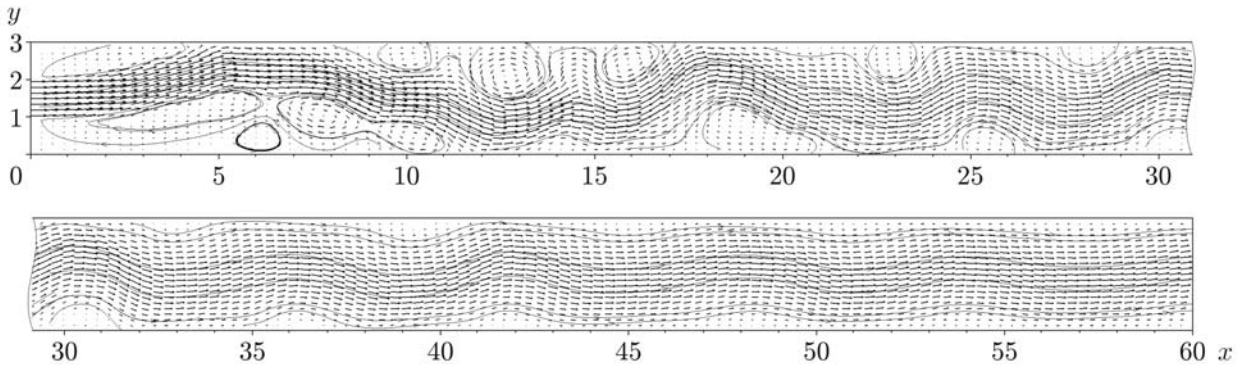

Fig. 3. Flow velocity vectors and streamlines at the time $t = 400$ at $\mathrm{Re} = 600$.

zones. Arising alternatively on the top and on the bottom of the channel, these zones deflect the flow upward and downward, respectively. At $\mathrm{Re} > 700$, the reverse process is observed: the zones with the decelerated flow near the wall periodically transform into vortices, thus, forming separation regions with reverse flows. This situation is caused by the influence of the increasing Reynolds number and no-slip conditions on the flow. The effect of viscosity near the wall, also caused by no-slip conditions, is manifested in deceleration of the gas, which lags behind the main flow as the Reynolds number and inertial forces increase. As a result, the streamlines are shifted, and separations with reverse flows occur. As a whole, however, the flow oscillations decrease with increasing the x coordinate,

TABLE 1

Maximum Distances on the Upper and Lower Walls Reached by the Vortices

Re	$x_{\max}\|_{y=3}$	$x_{\max}\|_{y=0}$
600	41.5	40.90
700	42.8	45.70
800	45.2	47.40
900	50.9	53.75

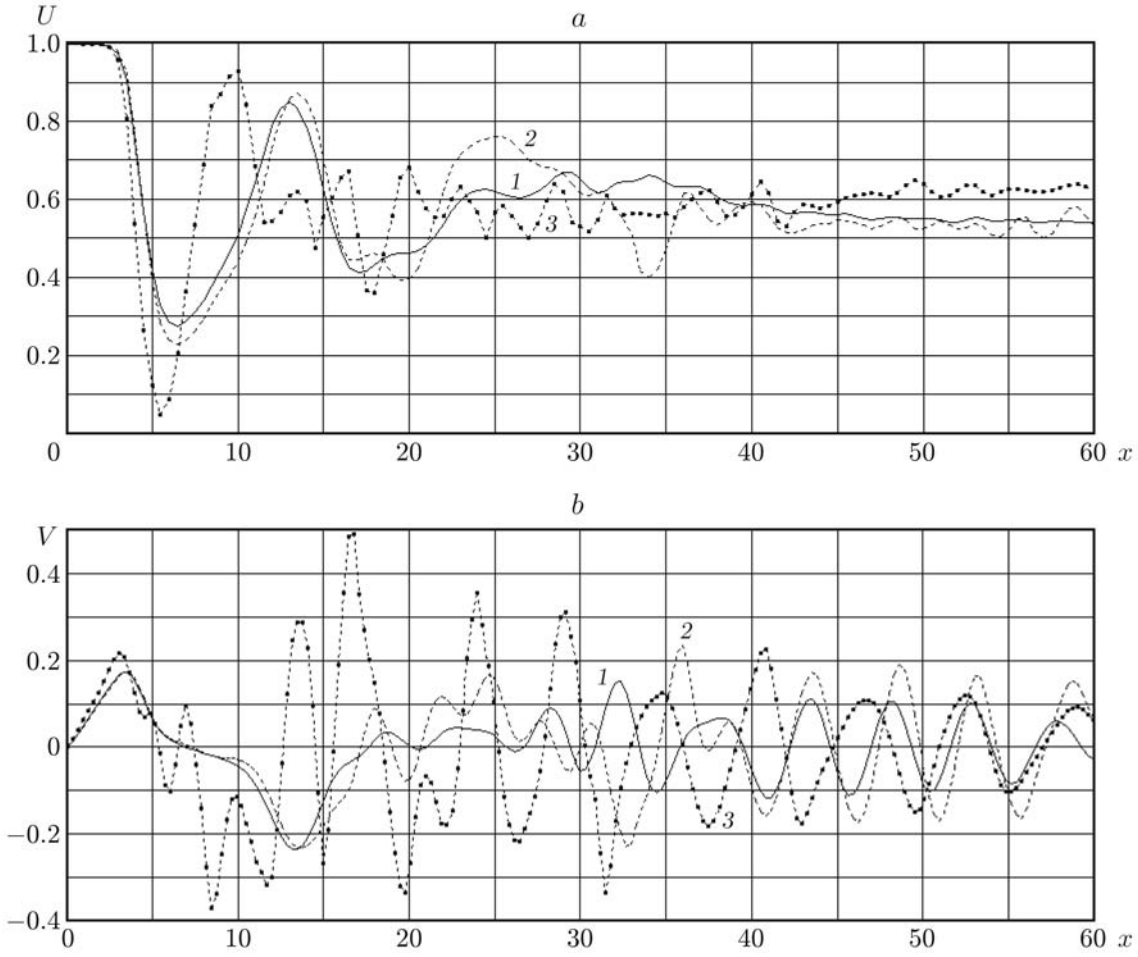

Fig. 4. Streamwise (a) and vertical (b) components of the flow velocity vector along the channel at the time $t = 400$ at $y = 1.5$, $z = 0$, and different Reynolds numbers: Re = 430 (1), 500 (2), and 600 (3).

though the flow remains essentially unsteady at $x = 60$. As the Reynolds number increases, the separation regions with reverse flows (vortices) penetrate deeper inward the channel. The maximum distances $x_{\max}$ on the upper and lower walls, which are reached by the vortices at different Reynolds numbers, are summarized in Table 1.

As the Reynolds number increases, the vortices moving along the channel change their shape. At Re = 700, the vortices are shaped as ellipses extended in the x direction; at Re > 700, the vortices begin to extend in the y direction; finally, at Re = 900, the vortices acquire the shape of ellipses extended in the y direction.

Figure 4 shows the streamwise and vertical components of the velocity vector as functions of the x coordinate at $y = 1.5$, $z = 0$, and different values of the Reynolds number at the time $t = 400$. It is seen that the streamwise component U becomes stabilized with increasing x. The vertical component V of the flow velocity vector at $y = 1.5$

TABLE 2

Maximums ($U_{\max}$ and $V_{\max}$) and Minimums ($U_{\min}$ and $V_{\min}$) of the Streamwise and Vertical Components of the Flow Velocity Vector on the Axis of Symmetry of the Flow

Re	$U_{\max}$	$U_{\min}$	$V_{\max}$	$V_{\min}$
430	0.998	0.269	0.174	−0.248
500	0.999	0.225	0.319	−0.302
600	1.036	0.020	0.557	−0.543
700	1.070	−0.087	0.663	−0.789
800	1.096	−0.184	0.753	−0.893
900	1.117	−0.279	0.817	−0.975

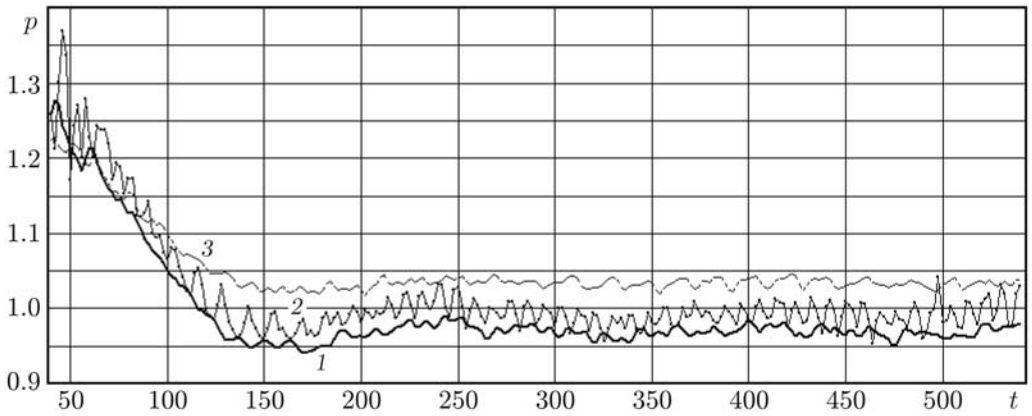

Fig. 5. Pressure versus the dimensionless time at $y = 1.5$, $z = 0$, and $\mathrm{Re} = 600$ at different points on the channel axis: $x = 1$ (1), 10 (2), and 45 (3).

and $z = 0$ is an oscillating function of the x coordinate. With increasing Reynolds number, these oscillations are also enhanced, whereas the amplitude of oscillations of V decreases with increasing the x coordinate. Nevertheless, these oscillations are still fairly significant at $x = 60$ and $\mathrm{Re} = 600$. A similar character of the behavior of U and V is observed at $\mathrm{Re} > 600$. Though the maximum deviations of the U and V components also increase with increasing Reynolds number, they do not exceed a certain level (Table 2). Similar tendencies are observed in the behavior of $U_{\min}$ and $V_{\min}$.

The most significant changes in U and V are observed in the separation regions in the vicinity of the left boundary of the channel.

Figure 5 shows the time evolution of pressure at $\mathrm{Re} = 600$ at three points of the channel: in the vicinity of the left boundary ($x = 1$), at $x = 10$ and 45. It is seen that the global behavior of all curves is similar. The pressure decreases first and then (at $t > 140$) becomes almost constant. Local variations of pressure stay within 3%. Similar results are also obtained for different values of the Reynolds number.

Figure 6 shows the shear friction stress ($\tau|_{\substack{y=0\\y=3}} = \partial U/\partial y$) on the upper and lower walls of the channel versus the x coordinate for different Reynolds numbers at the time $t = 500$. Under unsteady conditions, hydromechanical parameters are oscillating functions of the x coordinate with the amplitude of oscillations gradually decaying in the downstream direction.

It was shown [2] that the length of the lower separation region ($x \approx 12$) becomes significantly greater than the length of the upper separation region ($x \approx 4$) if the flow is deflected upward in the vicinity of the left boundary of the channel. A similar picture is observed at $\mathrm{Re} = 400$–900, but the separation regions become unsteady in this case. In addition, these regions lose stability with increasing Reynolds number, and the vortices are shed in the downstream direction. It is seen in Fig. 6 that the separation region on the lower wall loses its stability earlier, and the curve at $\mathrm{Re} = 500$ does not intersect the axis in the area of the lower separation region ($x \approx 12$). This testifies that the flow changes its direction several times near the lower wall in the vicinity of the channel entrance at $\mathrm{Re} > 500$. At $\mathrm{Re} < 500$, the flow the flow has a rather large stable separation region on the lower wall ($x \approx 14$), though this region is unsteady. In the corresponding region on the upper wall ($x \approx 4$), the friction stress curves

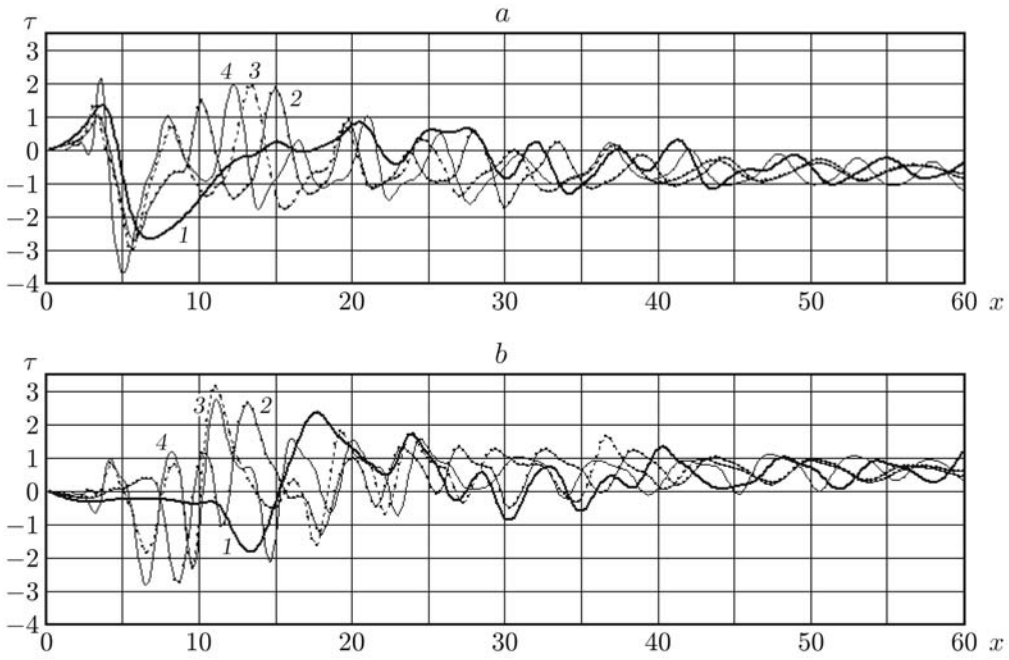

Fig. 6. Friction stress on the channel walls at the time $t = 500$ for different Reynolds numbers: (a) upper wall ($y = 3$); (b) lower wall ($y = 0$); Re = 500 (1), 600 (2), 700 (3), and 900 (4).

do not intersect the axis up to the Reynolds number Re = 900. Thus, we can conclude that the upper separation region is more stable than the lower separation region.

The shear friction stresses have different signs in the vicinity of the right boundary of the channel: the friction stress is negative on the upper boundary and positive on the lower boundary, i.e., there are no intersections with the axis. The absolute values of the shear friction stresses are approximately identical.

This work was supported by the Russian Foundation for Basic Research (Grant No. 07-08-96044-r_ural_a) and by the Grant for Young Researchers and Ph. D. Students of the Ural Division of the Russian Academy of Sciences.

REFERENCES

1. A. M. Lipanov and S. A. Karskanov, "Stabilization and evolution of parameters of a symmetric laminar flow in a plane channel with sudden expansion," *J. Appl. Mech. Tech. Phys.*, **48**, No. 1, 27–33 (2007).
2. A. M. Lipanov and S. A. Karskanov, "Investigation of steady laminar flows with an initial disturbance," *J. Appl. Mech. Tech. Phys.*, **49**, No. 3, 354–361 (2008).
3. N. E. Kochin, I. A. Kibel, and N. V. Rose, *Theoretical Hydrodynamics* [in Russian], Fizmatgiz, Moscow (1963).
4. A. T. Fedorchenko, "Numerical study of unsteady subsonic viscous gas flows in a suddenly expanding plane channel," *Izv. Ross. Akad. Nauk, Mekh. Zhidk. Gaza*, No. 4, 32–41 (1988).
5. A. M. Lipanov, Yu. F. Kisarov, and I. G. Klyuchnikov, *Numerical Experiment in Classical Hydromechanics of Turbulent Flows* [in Russian], Izd. Ural. Otd. Ross. Akad. Nauk, Ekaterinburg (2001).